Development of Doubly Salient Permanent Magnet Motors for Electric Vehicles

Ying Fan [1] and K. T. Chau [2]

[1] *Department of Electrical and Electronic Engineering, University of Hong Kong, yfan@eee.hku.hk*
[2] *Department of Electrical and Electronic Engineering, University of Hong Kong, ktchau@eee.hku.hk*

Abstract

In this paper, various motors for electric vehicles (EVs) are briefly reviewed. Then the development of doubly salient permanent magnet (DSPM) motors is presented, with emphasis on design and operation, torque production, comparison of pole numbers and discussion of operating modes. An 8/6-pole DSPM motor is designed and built for exemplification. Experimental results of the prototype are given to verify the theoretical analysis, hence confirming that DSPM motors are attractive for modern EVs.

Keywords

doubly salient, permanent magnet motor, electric vehicle

1. INTRODUCTION

In a world where environmental protection and energy conservation are growing concerns, the development of electric vehicle (EV) technology has taken on an accelerated pace to fulfill these needs.

Because EVs provide emission-free from the point of use, they can reduce the air pollution in crowded urban area. With the growing concern for air quality, some cities have set zero-emission zones and have enforced strict emission regulations to encourage the use of EVs [Chan et al., 1997]. EVs in America, Europe, Asia, and most of the world are being developed very quickly.

Electric propulsion is to interface electric supply with vehicle wheels, transferring energy in either direction as required, with high efficiency, under control of the driver at all times. From the functional point of view, an electric propulsion system can be divided into two parts - electrical and mechanical. The electrical part includes the motor, power converter, and electronic controller. On the other hand, the mechanical part consists of the transmission device and wheels. Sometimes, the transmission device is optional. The boundary between electrical and mechanical parts is the air-gap of the motor, where electromechanical energy conversion is taking place. Therefore, the development of EV motors plays a very important role. The purpose of this paper is to review various EV motors and hence to present the development of doubly salient permanent magnet (DSPM) motors for EVs.

2. REVIEW OF EV MOTORS

Electric motors have been available for over a century. The evolution of motors, unlike that of electronics and computer science, has been long and slow. Nevertheless, the development of motors is continually fueled by high-energy permanent magnets (PMs), sophisticated motor topologies, and powerful computer-aided design (CAD) techniques. As shown in Figure 1, those motors with dashed frame applicable to electric propulsion can be classified as two main groups, namely the commutator motors and commutatorless motors.

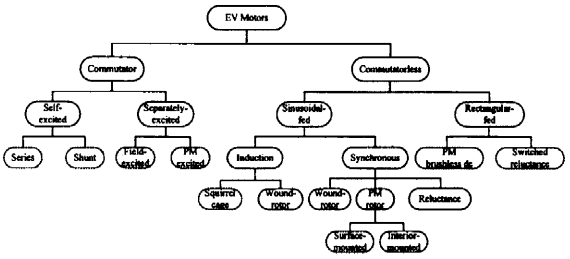

Fig. 1 Classification of EV motors

PMs provide motors with lifelong excitation. The only outlay is the initial cost which is reflected by the price of motors. Apart from ferrites, alnico, and samarium-cobalt (Sm-Co), neodymium-iron-boron (Nd-Fe-B) PMs have been introduced. Because of their highest remanence and coercivity as well as reasonable low cost, Nd-Fe-B PMs have promising applications to motors. In fact, adopting these "super magnets," a number of new motor topologies with high power density and high efficiency have recently been developed [Miller, 1989].

Traditional dc commutator motors, loosely named as dc motors, have been prominent in EV propulsion. Their control principle is simple. By replacing the field winding and pole structure with high-energy PMs, PM dc motors permit a considerable reduction in stator diameter. Owing to the low permeability of PMs, armature reaction is usually reduced and commutation is improved. However, the principal problem of dc motors

arises from their commutators and brushes which make them less reliable and unsuitable for maintenance-free operation.

Recent technological developments have pushed ac motors to a new era, leading to definite advantages over dc motors: higher efficiency, higher power density, lower cost, more reliable, and almost maintenance free. As high reliability and maintenance-free operation are prime considerations in EV propulsion, ac induction motors are attractive. However, conventional control of induction motors such as variable-voltage variable-frequency (VVVF) cannot provide the desired performance of EVs [Chan et al., 1987]. One major reason is due to the nonlinearity of its dynamic model with coupling between direct and quadrature axes. With the advent of the microcomputer era, the principle of field-oriented control (FOC) of induction motors has been accepted [Chan et al., 1990].

By replacing the field winding with high-energy PMs, PM synchronous motors can eliminate conventional brushes, slip-rings, and field copper losses. As these motors are essentially traditional ac synchronous motors with sinusoidal-distributed windings, they can run from a sinusoidal or PWM supply without electronic commutation. When PMs are mounted on the rotor surface, they behave as non-salient synchronous motors because the permeability of PMs is similar to that of air. On the other hand, by burying PMs inside the magnetic circuit of the rotor, the saliency causes an additional reluctance torque which leads to provide a wide speed range at constant power operation [Chan et al., 1996].

By inverting the stator and rotor of PM dc motors, rectangular-fed ac motors, so-called PM brushless dc motors, are generated. The most obvious advantage of these motors is the removal of brushes, leading to the elimination of many problems associated with brushes. Another advantage is the ability to produce a larger torque at the same peak current and voltage because of the interaction between rectangular current and rectangular magnetic field [Chan et al., 1993 and Chan et al., 1994]. Moreover, the brushless configuration allows more cross-sectional area available for the armature winding, thus facilitating the conduction of heat through the frame and, hence, increasing the electric loading and power density. Although their configurations are very similar to those of PM synchronous motors, there is a distinct difference in that PM brushless dc motors are fed by rectangular ac wave, while PM synchronous motors are fed by sinusoidal or PWM ac wave.

Switched reluctance motors, though the principle of which has been known for over a century, have seen a revival of interest in recent years. Basically, they are direct derivatives of single-stack variable-reluctance stepper motors, in which the current pulses are phased relative to the rotor position to optimize operation in the continuous rotation mode. Similar to PM brushless dc motors, they usually require shaft position sensors. However, switched reluctance motors suffer from the same excitation penalty as induction motors, and cannot attain the efficiency or power density of PM ac motors.

Recently, a research direction has been identified on the development of PM hybrid motors for EV applications. In principle, there are many PM hybrids in which three of them have been actively investigated, namely the PM and reluctance hybrid, the PM and hysteresis hybrid, and the PM and field-winding hybrid. Firstly, by embedding PMs inside the magnetic circuit of rotor, the PM synchronous motor can easily incorporate both PM torque and synchronous reluctance torque. On the other hand, by incorporating PMs into the SR structure, another PM and reluctance hybrid is generated which is so-called DSPM motor [Liao et al., 1995; Cheng et al., 2000]. Recent development of this DSPM motor has shown that it is of high efficiency, high power density and wide speed range [Cheng et al., 2003]. Secondly, another PM hybrid motor, incorporating both PM torque and hysteresis torque, has been introduced [Rahman et al., 1997]. By inserting PMs into the slots at the inner surface of the hysteresis ring, this PM hysteresis hybrid motor can offer unique advantages such as high starting torque as well as smooth and quiet operation for EV applications. Thirdly, another PM hybrid motor has been developed for EVs, which comprises of both PMs in the rotor and a dc field winding in the inner rotor [Chan et al., 1996]. By controlling the direction and magnitude of the dc field current, the air-gap flux of this motor can be flexibly adjusted, hence the torque speed characteristics can be easily shaped to meet the special requirements for EV propulsion.

3. DESIGN OF DSPM MOTORS

By following the approach described in [Cheng et al., 2001], the design equation of DSPM motors can be derived as:

$$D_{si}^2 l_e = \frac{P_2}{\frac{0.87\pi^2}{120}\frac{p_r}{p_s} k_d k_e k_i A_s B_\delta n_s \eta} \tag{1}$$

where D_{si} is the inner diameter of stator, l_e is the stack length, P_2 is the output power, P_r and P_s are the rotor and stator pole numbers, respectively, A_s is the electric loading of stator, B_δ is the airgap flux density, n_s is the rated speed in rpm, η is the motor efficiency, k_d is the flux leakage factor, $k_e = U/E$ is the ratio of applied voltage to back EMF, $k_i = I_{ni}/I_{rms}$ is the ratio of current magnitude to its rms value.

There is a wide range of possible combinations of phase number, stator pole number and rotor pole number that can be chosen for DSPM motor design. In accordance with the basic operating principle of DSPM motors, the general relationships among the stator pole number p_s, rotor pole number p_r and phase number m are given by:

$$\begin{cases} p_s = 2mk \\ p_r = p_s \pm 2k \end{cases} \tag{2}$$

where k is a positive integer. When the motor runs at the speed of n, the commutating frequency of any phase is given by:

$$f_{ph} = p_r n/60 \tag{3}$$

To minimize the switching frequency and hence the iron losses in poles and yokes as well as the loss in power switches, the number of rotor poles should be selected as small as possible. Therefore, the number of rotor poles is usually less than that of stator poles. To make the motor capable of starting itself in either forward or reverse direction, the phase number should be equal to or greater than three.

Figure 2 shows the cross section of both the four-phase 8/6-pole and three-phase 6/4-pole DSPM motors with stationary PMs. It can be seen that the rotor of DSPM motors is the same as that of switched reluctance (SR) motors. The stator structure is also similar to that of SR motors except two pieces of PMs are inserted in the stator core. The Nd-Fe-B PM material is generally adopted since it can offer high energy content and almost linear demagnetizing characteristics. Since the stator can be easily cooled by natural or forced cooling, irreversible demagnetization is avoided. Hence DSPM motors are able to work at high temperature, facilitating their applications to EVs.

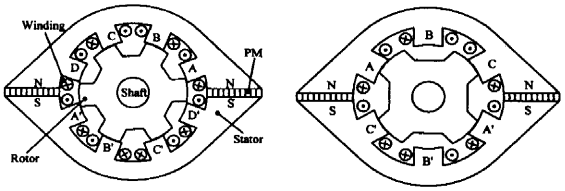

(a) 8/6-pole (b) 6/4-pole

Fig. 2 Cross section of DSPM motors

When magnet fringing is negligible, the PM flux linkage ψ_{pm} has a linear variation. Figure 3 shows the theoretical ψ_{pm} waveform and the corresponding stator phase current i_s waveform.

The terminal voltage equation for an active phase winding is given by:

$$u = e + ri_s = \frac{d\psi}{dt} + ri_s \tag{4}$$

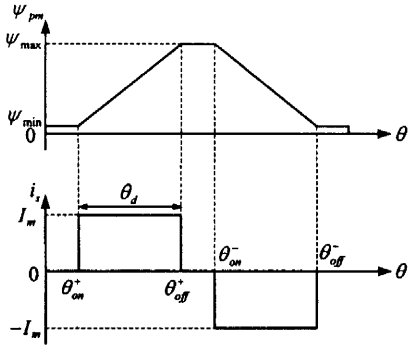

Fig. 3 Theoretical waveforms of PM flux linkage and stator phase current

where u is the phase voltage, r is the phase resistance, i_s is the stator phase current, ψ is the flux linkage and e is the back EMF. The flux linkage can be regarded as the sum of the flux linkages from both PMs and the stator winding as given by:

$$\psi = \psi_{pm} + Li_s \tag{5}$$

where ψ_{pm} is the flux linkage from PMs, L is the phase inductance, and Li_s is the flux linkage from the stator winding. Hence, the back EMF is given by:

$$e = \frac{d\psi}{dt} = \frac{d\psi_{pm}}{dt} + L\frac{di_s}{dt} + i_s\frac{dL}{dt} \tag{6}$$

Neglecting the copper and iron losses, the input power can be expressed as:

$$\begin{aligned} P = ei_s &= i_s\frac{d\psi_{pm}}{dt} + i_s L\frac{di_s}{dt} + i_s^2\frac{dL}{dt} \\ &= \frac{d}{dt}\left(\frac{1}{2}Li_s^2\right) + \left(i_s\frac{d\psi_{pm}}{d\theta} + \frac{1}{2}i_s^2\frac{dL}{d\theta}\right)\omega_r \\ &= \frac{d}{dt}W_w + T\omega_r \end{aligned} \tag{7}$$

where θ is the rotor position, and W_w is the armature reaction field energy as defined by:

$$W_w = \frac{1}{2}Li_s^2 \tag{8}$$

This field energy is very small because of the low inductance in DSPM motors. Hence, the electromagnetic torque per phase can be expressed as the sum of two components, namely the PM torque and reluctance torque:

$$T = i_s\frac{d\psi_{pm}}{d\theta} + \frac{1}{2}i_s^2\frac{dL}{d\theta} = T_{pm} + T_r \tag{9}$$

where T is the electromagnetic torque, $T_{pm} = i_s\, d\psi_{pm}(\theta)/d\theta$ is the PM torque component due to the interaction between PM flux linkage and arma-

ture current, and $T_r = 1/2 i_s^2 \, dL(\theta)/d\theta$ is the reluctance torque component due to the variation of inductance.

4. COMPARISON OF DSPM MOTORS

Based on the same physical dimensions, the design data of both 8/6-pole and 6/4-pole DSPM motors are listed in Table 1. Provided that their surface current densities are the same, the output power capability P_o of the 6/4-pole motor operating at 1500 rpm is found to be 820 W as shown in Figure 4. Comparing with the 892 W offered by the 8/6-pole one, the power density of the 8/6-pole motor is 9% higher than that of the 6/4-pole one. Moreover, it can be observed that the 8/6-pole motor can achieve higher output power and wider speed range while offering lower stator phase current I_s than the 6/4-pole one.

Table 1 Design data of 8/6-pole and 6/4-pole DSPM motors

	8/6-pole	6/4-pole
Stator outer diameter (mm)	128	128
Stator inner diameter (mm)	75	75
Stack length (mm)	75	75
Air-gap length (mm)	0.45	0.45
Stator pole number	8	6
Rotor pole number	6	4
Stator pole arc (°)	22	30
Rotor pole arc (°)	26	36
Stator pole depth (mm)	13	13
Rotor pole depth (mm)	10	10
Number of turns/phase	220	250
Rated speed (rpm)	1500	1500
Magnet remanence (T)	1.045	1.045
Magnet volume (cm^3)	33.3	33.3
Length of windings (m)	189	181

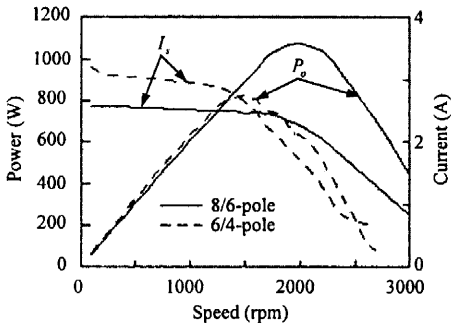

Fig. 4 Comparison of power and current

Furthermore, the torque waveforms of these two motors operating at their maximum output power and rated speed are shown in Figure 5. Under the same operating conditions and without employing any particular current control methods, it can be found that the torque ripple of the 6/4-pole motor is significantly larger than that of the 8/6-pole one. By defining the torque ripple factor as:

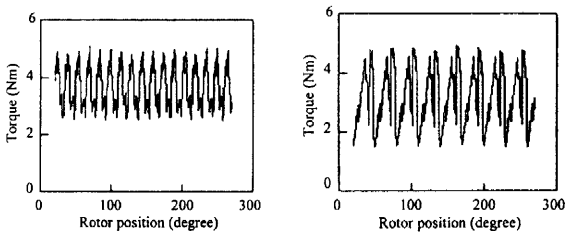

(a) 8/6-pole (b) 6/4-pole

Fig. 5 Comparison of torque ripples

$$k_t = \frac{T_{max} - T_{min}}{T_{max} + T_{min}} \times 100\% \qquad (10)$$

where T_{max} and T_{min} are the maximum and minimum torque values. The corresponding k_t for the 6/4-pole and 8/6-pole motors are 33% and 22.5%, respectively. The 8/6-pole DSPM motor uses the same amount of materials as the 6/4-pole. Although the corresponding length of windings is longer by 8 m, the cost of its windings is lower than that of the 6/4-pole one because of its smaller cross-sectional area under lower current rating. Moreover, a typical cost comparison of their power converters is shown in [Chau et al., 1999]. It can be found that the higher the power rating, the better the cost effectiveness of the power converter for the 8/6-pole DSPM motor.

The above comparison has shown that the 8/6-pole DSPM motor takes advantages over the 6/4-pole counterpart, namely higher power density, wider speed range, less torque ripple and lower current magnitude.

5. OPERATING MODES OF DSPM MOTORS

To supply the DSPM motor, a bipolar converter topology is preferred so as to make the bi-directional current operation possible. Hence, there are two converter topologies in which the phase current can be control individually for bi-directional operation of the 8/6-pole DSPM motor, namely the full-bridge converter and the half-bridge converter with split capacitors.

The 8/6-pole DSPM motor can be controlled to operate at the square-wave current mode without rotor skewing and the sinusoidal current mode with rotor skewing. To minimize the torque ripple, the sinusoidal current one is adopted in such a way that the phase current is controlled to synchronize with the phase back EMF. The skewing angle of the rotor is specially selected at $\alpha = 21^\circ$. This value is the simulation result aiming to make $dL_{sk}/d\theta$ and $d\psi_{sk}/d\theta$ nearly sinusoidal as shown in Figure 6, where L_{sk} and ψ_{sk} are the phase inductance and flux link-

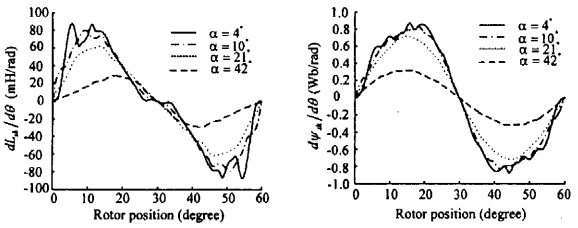

(a) $dL_{sk}/d\theta$ (b) $d\psi_{sk}/d\theta$

Fig. 6 Variation of motor parameters with the rotor skewing

age under rotor skewing, respectively.

To minimize the number of power switches, the half-bridge converter with split capacitors may be adopted. However, there is a possibility of voltage unbalancing between the two split capacitors. Although the connection between the center-point of these capacitors and the neutral of motor windings can be removed when $\theta_{on}^{-} = \theta_{on}^{+} + \theta_{cr}/2$ and $\theta_{off}^{-} = \theta_{off}^{+} + \theta_{cr}/2$, the four-phase winding will no longer be controlled individually [Cheng et al., 2003].

Further inspecting the characteristics and the control logic of the 8/6-pole DSPM motor discloses that there is a possibility of this motor running as a two-phase motor. As shown in Figure 7, the windings A and C and the windings B and D are reversibly connected in series. It can be found that the two-phase full-bridge converter has the same number of power switches as the four-phase half-bridge converter. Therefore, its phase current can be controlled independently without requiring split capacitors.

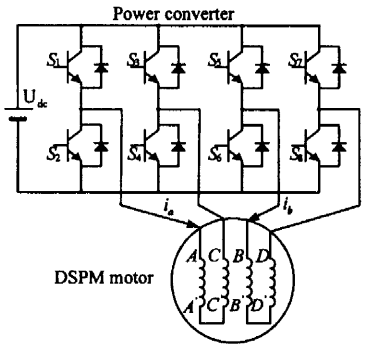

Fig. 7 Two-phase 8/6-pole DSPM motor using full-bridge converter

Furthermore, its voltage rating of power switches is half that of the half-bridge converter. Figure 8 shows the control block of this two-phase 8/6-pole DSPM motor. It has two closed loops which are the current loop for regulating the phase current and the speed loop for regulating the motor speed, respectively. Based on the above analysis, the DSPM motor drive is identified to be attractive for EV propulsion.

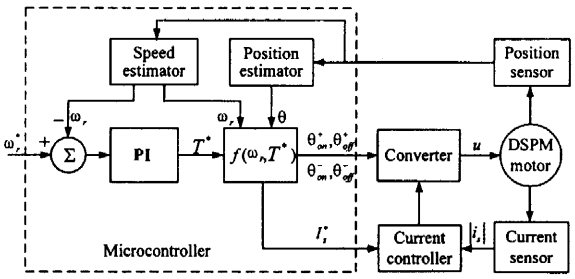

Fig. 8 Control block diagram of two-phase 8/6-pole DSPM motor

6. RESULTS AND VERIFICATION

The aforementioned two-phase 8/6-pole DSPM motor is computer simulated and experimentally tested. Figure 9 shows the simulated average torque and torque ripple factor at the rated current versus the rotor skewing angle. It can be seen that the rotor skewing angle of 21° is an optimal compromise between the average torque and the torque ripple factor. Also, Figure 10 shows the simulated average torque and torque ripple factor at the rated current versus the phase shifting angle between the back EMF and current. It can be seen that 0° is the best choice, which agrees with the theoretical derivation.

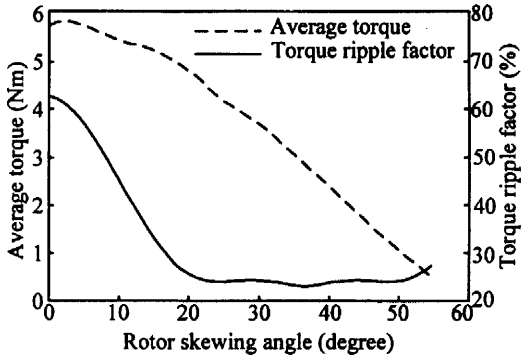

Fig. 9 Influence of rotor skewing angle

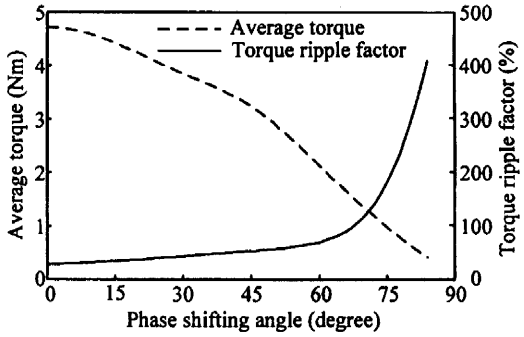

Fig. 10 Influence of phase shifting angle

Figure 11 shows the simulated no-load EMF at rated load. As expected, it is very sinusoidal. On the other hand, Figure 12 shows the simulated waveforms of phase current and torque of the DSPM motor. As expected,

the current waveform is very sinusoidal and the torque waveform exhibits small torque ripple. Also, it can be seen that the torque waveform swings between 4.1 Nm and 5.2 Nm under the rated load of 4.7 Nm. By using (10), it results k_t = 11.8% which is 10.7% lower than that under four-phase operation. Therefore, the two-phase operation can significantly reduce the torque ripple occurred at four-phase operation.

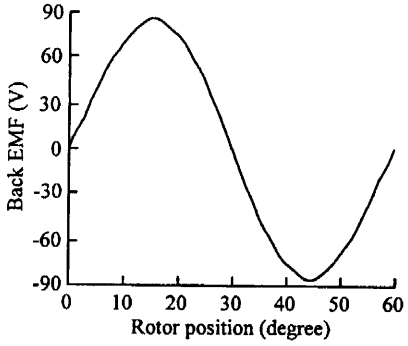

Fig. 11 Simulated no-load EMF at rated speed

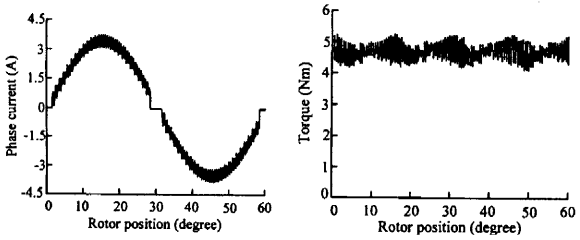

(a) Phase current (b) Torque

Fig. 12 Simulated waveforms at rated load during two-phase operation

An 8/6-pole DSPM motor prototype, with the ratings of 750 W and 1500 rpm, is designed and built for verification. An IGBT based converter and a microcontroller-based controller are also implemented to drive the motor. In order to directly measure the torque ripple, a transient torque transducer is mounted between the motor and the dynamometer which is the load of the two-phase 8/6-pole DSPM motor. The stator current is also measured by a Hall effect current sensor.

Figure 13 shows the measured no-load EMF waveform at the rated speed, indicating that the air-gap flux of the motor is very sinusoidal. It can be found that it closely agrees with the simulated waveform shown in Figure 11. Also, both the phase current and torque waveforms are measured at the rated load. Figure 14 confirms that the measured current is very sinusoidal and the measured torque ripple is minimal.

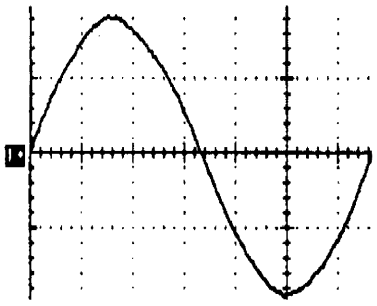

Fig. 13 Measured no-load EMF at rated speed (50 V/div, 2.5 ms/div)

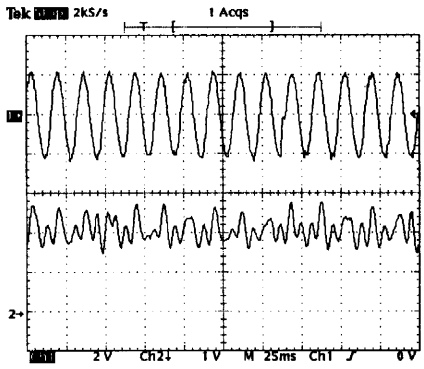

Fig. 14 Measured current and torque at rated load (3.3 A/div, 2.3 Nm/div, 25 ms/div)

7. CONCLUSION

In this paper, various EV motors have been briefly reviewed, and the development of DSPM motors for EVs has been discussed. The basic configuration and operating principle of DSPM motors are described. The design of a new DSPM motor is presented and the corresponding output power equation is analytically derived. Furthermore, the 8/6-pole and 6/4-pole DSPM motors are compared in terms of their power density and torque ripple factor. Two operating modes are presented in which the two-phase one is identified to realize the minimum torque ripple. An 8/6-pole DSPM motor is designed and built for exemplification. Experimental results of the prototype are given to verify the theoretical analysis. In summary, the DSPM motor offers the following advantageous features:

- Simple, rugged and high speed capability.
- High power density and high efficiency.
- Low inertia and fast response.
- PMs are located in stator which can avoid the irreversible demagnetization due to over-temperature.
- High energy conversion ration and small VA rating of power converter as well as the motor.

These features make the DSPM motor very competitive for EV propulsion.

Acknowledgements

This work was supported and funded in part by the Hong Kong Research Grants Council, and the Committee on Research and Conference Grants of the University of Hong Kong.

References

Chan, C. C., and K. T. Chau, An Advanced Permanent Magnet Motor Drive System for Battery-powered Electric Vehicles, *IEEE Transactions on Vehicular Technology*, Vol. 45, No. 1, 180-188, 1996.

Chan, C. C., and K. T. Chau, An Overview of Power Electronics in Electric Vehicles, *IEEE Transactions on Industrial Electronics*, Vol. 44, No. 1, 3-13, 1997.

Chan, C. C., and W. C. Lo, Control Strategy of PWM Inverter Drive System for Electric Vehicles, *IEEE Transactions on Industrial Electronics*, Vol. 34, No. 4, 447-456, 1987.

Chan, C. C., K. T. Chau, J. Z. Jiang, W. Xia, M. Zhu, and R. Zhang, Novel Permanent Magnet Motor Drives for Electric Vehicles, *IEEE Transactions on Industrial Electronics*, Vol. 43, No. 2, 331-339, 1996.

Chan, C. C., J. Z. Jiang, G. H. Chen, and K. T. Chau, Computer Simulation and Analysis of a New Polyphase Multipole Motor Drive, *IEEE Transactions on Industrial Electronics*, Vol. 40, No. 6, 570-576, 1993.

Chan, C. C., J. Z. Jiang, G. H. Chen, X. Y. Wang, and K. T. Chau, A Novel Polyphase Multipole Square-wave Permanent Magnet Motor Drive for Electric Vehicles, *IEEE Transactions on Industry Applications*, Vol. 30, No. 5, 1258-1266, 1994.

Chau, K. T., M. Cheng, and C. C. Chan, Performance Analysis of 8/6-Pole Doubly Salient Permanent Magnet Motor, *Electric Machines and Power Systems*, Vol. 27, No. 10, 1055-1067, 1999.

Chan, C. C., W. S. Leung, and C. W. Ng, Adaptive Decoupling Control of Induction Motor Drives, *IEEE Transactions on Industrial Electronics*, Vol. 37, No.1, 41-47, 1990.

Cheng M., K. T. Chau, C. C. Chan, and Q. Sun, Control and Operation of a New 8/6-Pole Doubly Salient Permanent-Magnet Motor Drive, *IEEE Transactions on Industry Applications*, Vol. 39, No.5, 1363-1370, 2003.

Cheng M., K. T. Chau, and C. C. Chan, Design and Analysis of a New Doubly Salient Permanent Magnet Motor, *IEEE Transactions on Magnetics*, Vol. 37, No. 4, 3012-3020, 2001.

Cheng M., K. T. Chau, C. C. Chan, E. Zhou and X. Huang, Nonlinear Varying-network Magnetic Circuit Analysis for Doubly Salient Permanent Magnet Motors, *IEEE Transactions on Magnetics*, Vol. 36, No. 1, 339-348, 2000.

Cheng M., K. T. Chau, and C. C. Chan, New Split-winding Doubly Salient Permanent Magnet Motor Drive, *IEEE Transactions on Aerospace and Electronic Systems*, Vol. 39, No. 1, 202-210, 2003.

Liao, Y., F. Liang, and T. A. Lipo, A Novel Permanernt Magnet Motor With Doubly Salient Structure, *IEEE Transactions on Industry Applications*, Vol. 31, No. 7, 1069-1078, 1995.

Miller, T. J. E., *Brushless Permanent-Magnet and Reluctance Motor Drives*, London, U.K.: Oxford Univ. Press, 1989.

Rahman, M. A., and R. F. Qin, A Permanent Magnet Hysteresis Hybrid Synchronous Motor for Electric Vehicles, *IEEE Transactions on Industrial Electronics*, Vol. 44, No. 1, 46-53, 1997.

(Received May 13, 2005; accepted June 15, 2005)